

Quantum criticality of the Ohmic spin-boson model in a high dense spectrum: symmetries, quantum fluctuations and correlations

Xiaohui Qian, Congzhi Zeng, Nengji Zhou*

Department of Physics, Hangzhou Normal University, Hangzhou 311121, China, PRC

Abstract

Study of dissipative quantum phase transitions in the Ohmic spin-boson model is numerically challenging in a dense limit of environmental modes. In this work, large-scale numerical simulations are carried out based on the variational principle. The validity of variational calculations, spontaneous breakdown of symmetries, and quantum fluctuations and correlations in the Ohmic bath are carefully analyzed, and the critical coupling as well as exponents are accurately determined in the weak tunneling and continuum limits. In addition, quantum criticality of the Ohmic bath is uncovered both in the delocalized phase and at the transition point.

Keywords: Critical phenomena, Spin-boson model, Numerical simulations, Open quantum systems

1. Introduction

Quantum phase transitions have been under intensive study over many decades in various correlated matters and light-matter interacting systems [1, 2, 3]. The accurate description of quantum effects is essential to the understanding of such quantum critical phenomena. As a paradigmatic minimal example, the spin-boson model (SBM) consisting of a spin-1/2 particle (two-level system) and a bosonic environment has attracted significant interest [4, 5, 6]. In spite of apparent simplicity, it catches the physics of a large

*Corresponding author.

Email address: zhounengji@hznu.edu.cn (Nengji Zhou)

range of different physical systems going from defects in solids and quantum thermodynamics [7, 8] to physical chemistry and biological systems [9, 10, 11]. It has also been used to study spontaneous emission in quantum optics [12], semiconducting quantum dots in nanocavities [13], trapped ions [14], quantum heat engines [15], and superconducting circuits [16]. The ground-state and dynamic properties of SBM have been extensively and persistently investigated with analytical and numerical approaches [17, 18, 19, 20, 21, 22]. In particular, the localized-delocalized ground-state transition and coherent-incoherent dynamic transition have been detected with the increase of the system-environment coupling [5, 4, 23]. Besides, many activities have also been devoted to the variants of SBM for richer phase diagrams [24, 25, 26, 27].

As the most well-known case, the Ohmic SBM has a linear spectral density function $J(\omega) \sim \alpha\omega^s$ with $s = 1$ to characterize the coupling between the system and the environment. The model can be mapped onto the anisotropic Kondo model and interacting resonant level model based on the equivalence between Fermi and Bose operators in one dimension [28]. Thus, the localized-delocalized phase transition of the Kosterlitz-Thouless type has been predicted, and the critical coupling is located around $\alpha = 1$ associated with the discontinuous jumps of the spin magnetization and entropy [5]. Different from the single-spin case, however, there was much debate among numerical works concerning the value of the critical coupling α_c for the two-impurity model, due to the lack of the analytical solution [29, 30, 31, 26]. Therefore, accurate determination of the transition point for the Ohmic SBM is still needed in numerical work to provide the methodological benchmark. Besides, the Ohmic SBM has been realized in recent experiments of superconducting quantum circuits wherein the spectral width of the reservoir is restricted [32, 16]. But the influence of the frequency range on the critical coupling α_c is still an open question.

A variety of numerical approaches have been employed to determine the nature of localized-delocalized transition and exact value of the critical coupling, e.g., numerical renormalization group (NRG), exact diagonalization, variational matrix product states, density-matrix renormalization group, quantum Monte Carlo (QMC), and variational method [33, 34, 35, 36, 24, 20]. While numerical results of critical couplings show considerable differences in the shallow sub-Ohmic regime with $s > 0.5$. For instance, the NRG value of α_c is greater than others by nearly 10 percent at $s = 0.9$, let alone the Ohmic case $s = 1$ [35, 36, 34]. Possible reason for the deviation is the numerical sensitivity of the phase transition nearby $s = 1$.

Furthermore, numerical calculations are exact only in the continuum limit corresponding to a high dense spectrum. In that case, however, the scale separation breaks down, and the truncation becomes unmanageable [20]. Accordingly, the linear extrapolation was used to determine the value of transition point [37]. But the linear dependence on the discretization parameter seems less convincing in the high dense spectrum. Very recently, quantum phase transitions of the Ohmic SBM in the continuum limit have been explored with the imaginary-time propagation [38, 39]. In spite of the critical coupling $\alpha \rightarrow 1^+$ has been arrived at directly, a detailed understanding of symmetries and quantum criticality of the Ohmic bath has been still lacking.

The pioneer variational work of the Ohmic SBM was based on the polaronic unitary transformation proposed by Silbey and Harris [17]. Later on, the variational polaron ansatz was improved by superposing more than one coherent states and removing the imposed symmetry constrain [18, 19, 40, 41, 42]. Recently, numerical variational method (NVM) has been developed based on systematic coherent-state decomposition of many-body ground state [25, 43]. Excellent accuracy and reliability of the NVM have been proved in tackling ground-state phase transitions and quantum dynamics in the sub-Ohmic regime [44, 45, 46, 47, 48]. However, the validity of the variational method for the Ohmic phase transition has not yet been demonstrated in the case of a high dense spectrum. Moreover, the attention in previous studies was mainly focused on the spin-related observations, especially for the spontaneous spin magnetization. In fact, bath observables provide a direct measurement of the quantum criticality intrinsic to the environment possessing many-body effects. But critical behaviors of quantum fluctuations and correlations in the Ohmic bath have not been clearly addressed so far.

In this article, quantum fluctuations and correlations in the Ohmic bath as well as the mechanism of spontaneous symmetry breaking are investigated with NVM for the Kosterlitz-Thouless transition. The transition point and exponents are accurately determined, and the validity of variational calculations is carefully examined. The rest of the paper is organized as follows. In section 2, the model and variational approach are described. In section 3, numerical results are presented for the spontaneous breakdown of symmetries, the characteristic of the ground-state wavefunction, and the quantum criticality of the Ohmic bath. Finally, conclusions are drawn in section 4.

2. Model and Method

The standard Hamiltonian of SBM can be written as

$$\hat{H} = \frac{\varepsilon}{2}\sigma_z - \frac{\Delta}{2}\sigma_x + \sum_k \omega_k b_k^\dagger b_k + \frac{\sigma_z}{2} \sum_k \lambda_k (b_k^\dagger + b_k), \quad (1)$$

where ε (Δ) denotes the energy bias (bare tunneling amplitude), b_k^\dagger (b_k) is the bosonic creation (annihilation) operator of the k -th bath mode with the frequency ω_k , σ_x and σ_z represent the Pauli spin-1/2 operators, and λ_k signifies the coupling amplitude between the system and environment. With the coarse-grained treatment based on the Wilson energy mesh [37, 33, 36, 25, 43], the values of λ_k and ω_k can be calculated by the continuous spectral density function $J(\omega) = 2\alpha\omega_c^{1-s}\omega^s\Theta(\omega_c - \omega) = \sum_k \lambda_k^2\delta(\omega - \omega_k)$ after partitioning the phonon frequency domain $[0, \omega_c]$ into M intervals $[\Lambda_k, \Lambda_{k+1}]\omega_c$ ($k = 0, 1, \dots, M - 1$),

$$\lambda_k^2 = \int_{\Lambda_k\omega_c}^{\Lambda_{k+1}\omega_c} dt J(t), \quad \omega_k = \lambda_k^{-2} \int_{\Lambda_k\omega_c}^{\Lambda_{k+1}\omega_c} dt J(t)t, \quad (2)$$

where M is the number of effective bath modes, and $\Theta(\omega_c - \omega)$ is the Heaviside step function. To simplify notations, hereafter we fix the Planck constant $\hbar = 1$ and the maximum frequency in the bath $\omega_c = 1$. Other model parameters, i.e., ε , Δ , and α , are then set to be dimensionless. A logarithmic discretization procedure with the parameter $\Lambda_k = \Lambda^{k-M}$ is usually adopted [49, 5, 18, 50], and the Wilson parameter $\Lambda \rightarrow 1$ is required for the Ohmic SBM (i.e., $s = 1$) in order to obtain an accurate quantum criticality of the Kosterlitz-Thouless transition. However, $\Lambda = 1.4 \sim 2.0$ was used in earlier numerical works [37, 29, 20] where the critical coupling deviates from the prediction $\alpha_c = 1$ by more than 10 percent due to the finite size effect. In this paper, main results are presented with $\Lambda = 1.01$. Additional simulations with $\Lambda = 1.02$ confirm that the effect of discretization is already sufficiently small.

In variational calculations, a systematic coherent-state expansion is used [25, 44, 47, 43, 26],

$$\begin{aligned} |\Psi\rangle &= |\uparrow\rangle \sum_{n=1}^N A_n \exp \left[\sum_{k=1}^M \left(f_{n,k} b_k^\dagger - \text{H.c.} \right) \right] |0\rangle_{\text{B}} \\ &+ |\downarrow\rangle \sum_{n=1}^N D_n \exp \left[\sum_{k=1}^M \left(g_{n,k} b_k^\dagger - \text{H.c.} \right) \right] |0\rangle_{\text{B}}, \end{aligned} \quad (3)$$

where H.c. denotes Hermitian conjugate, \uparrow (\downarrow) stands for the spin up (down) state, and $|0\rangle_{\text{b}}$ is the vacuum state of the bosonic bath. The variational parameters $f_{n,k}$ and $g_{n,k}$ represent the displacements of the coherent states correlated to the spin configurations $|\uparrow\rangle$ and $|\downarrow\rangle$, respectively, and A_n and D_n are weights of the coherent states. The subscripts n and k correspond to the ranks of the coherent superposition state and effective bath mode, respectively. The energy can be then expressed as $E = \mathcal{H}/\mathcal{N}$ using the Hamiltonian expectation $\mathcal{H} = \langle \Psi | \hat{H} | \Psi \rangle$ and norm of the wave function $\mathcal{N} = \langle \Psi | \Psi \rangle$. By minimizing the energy to search for the ground state $|\Psi_g\rangle$, the variational procedure entails a set of self-consistency equations

$$\frac{\partial \mathcal{H}}{\partial x_i} - E \frac{\partial \mathcal{N}}{\partial x_i} = 0, \quad (4)$$

where x_i is a certain variational parameter $f_{n,k}$, $g_{n,k}$, A_n , or D_n . For each set of the model parameters $(\alpha, M, \Lambda, \varepsilon)$, more than one hundred random initial states are used in simulations to find the ground state. Furthermore, simulated annealing algorithm is also employed to escape from metastable states.

Besides the ground-state energy E_g as well as the spin magnetization $\langle \sigma_z \rangle = \langle \Psi_g | \sigma_z | \Psi_g \rangle$, other observables related to the Ohmic bath are also investigated in the study of quantum phase transitions, which are the variances of phase-space variables ΔX_{b} and ΔP_{b} , correlation functions Cor_X and Cor_P , and average displacements \bar{f}_k and \bar{g}_k [20, 26, 43]. Noting $\langle \Psi_g | \hat{p}_k | \Psi_g \rangle = 0$, one has

$$\begin{aligned} \Delta X_{\text{b}} &= \langle \Psi_g | (\hat{x}_k)^2 | \Psi_g \rangle - \langle \Psi_g | \hat{x}_k | \Psi_g \rangle^2, \\ \Delta P_{\text{b}} &= \langle \Psi_g | (\hat{p}_k)^2 | \Psi_g \rangle, \\ \text{Cor}_X &= \langle \Psi_g | \hat{x}_k \hat{x}_l | \Psi_g \rangle - \langle \Psi_g | \hat{x}_k | \Psi_g \rangle \langle \Psi_g | \hat{x}_l | \Psi_g \rangle, \\ \text{Cor}_P &= \langle \Psi_g | \hat{p}_k \hat{p}_l | \Psi_g \rangle, \end{aligned} \quad (5)$$

where \hat{x}_k and \hat{p}_k represent quadrature operators for the phase-space variables, i.e., the position and momentum,

$$\hat{x}_k = (b_k + b_k^\dagger) / \sqrt{2}, \quad \hat{p}_k = i (b_k^\dagger - b_k) / \sqrt{2}, \quad (6)$$

and the subscripts k and l correspond to the k -th and l -th bath modes, respectively.

To capture the characteristic of the ground-state wavefunction, we introduce the average coherent-state weights

$$\bar{A} = \sqrt{\sum_{mn} A_m A_n F_{mn}}, \quad \bar{D} = \sqrt{\sum_{mn} D_m D_n G_{mn}}, \quad (7)$$

and the average displacement coefficients

$$\begin{aligned} \bar{f}_k &= \sum_{m,n} \frac{A_m A_n F_{mn} (f_{m,k} + f_{n,k})}{2\bar{A}^2}, \\ \bar{g}_k &= \sum_{m,n} \frac{D_m D_n G_{mn} (g_{m,k} + g_{n,k})}{2\bar{D}^2}, \end{aligned} \quad (8)$$

where the functions F_{mn} and G_{mn} are defined as

$$\begin{aligned} F_{mn} &= \exp \left[-\frac{1}{2} \sum_k (f_{m,k} - f_{n,k})^2 \right], \\ G_{mn} &= \exp \left[-\frac{1}{2} \sum_k (g_{m,k} - g_{n,k})^2 \right]. \end{aligned} \quad (9)$$

Finally, the symmetries of the ground state are also probed here. In the case of $\varepsilon = 0$ and $\Delta \neq 0$, the SBM may possess strong \mathbb{Z}_2 symmetry. Due to the competition between the tunneling and environmental dissipation, there exists a quantum phase transition separating a nondegenerate symmetric delocalized phase from a localized phase characterized by a doubly degenerate ground state. The projection operator from one branch to the other branch of the degenerate states is then introduced,

$$\hat{\mathcal{P}} = \sigma_x \exp \left[i\pi \sum_{k=1}^M b_k^\dagger b_k \right]. \quad (10)$$

The spontaneous breakdown of the \mathbb{Z}_2 symmetry can be described by the symmetry parameter defined as

$$\zeta = \langle \Psi_g | \hat{\mathcal{P}} | \Psi_g \rangle \Delta_E, \quad (11)$$

where Δ_E denotes a piecewise function of variable E_g , taking the values of 1 if $E_g(\Psi_g) = E_g(\hat{\mathcal{P}}\Psi_g)$, and 0 otherwise. Thereby the symmetry parameter is expected to be $\zeta = 1$ ($\zeta = 0$) for the delocalized (localized) phase,

corresponding to the ground state with (without) the \mathbb{Z}_2 symmetry. In the biased case, i.e., $\varepsilon \neq 0$, the vanishing value of ζ holds for any coupling α since $\Delta_E = 0$, indicating that the symmetry is always broken. Hence, $\zeta(\alpha)$ is a natural order parameter for quantum phase transitions associated with the spontaneous symmetry breaking.

3. Numerical results

The ground-state properties of the Ohmic SBM in a high dense spectrum are investigated with variational calculations in the weak tunneling limit, taking the setting of logarithmic discretization factor $\Lambda = 1.01$ and tunneling amplitude $\Delta = 0.01$ as an example. Theoretically, the number of effective bath modes $M \rightarrow \infty$ is required for the completeness of the environment. Considering the constraint available computational resources, a sufficiently large number $M = 1000$ is used in main results. Besides, the spectral exponent $s = 1$, number of coherent-superposition states $N = 6$, and energy bias $\varepsilon = 0$ are set unless noted otherwise. In numerical simulations, the statistical errors of the critical coupling and exponents are estimated by dividing the total samples into two subgroups. If the fluctuation in the frequency direction is comparable with or larger than the statistical error, it will be taken into account.

3.1. Spontaneous symmetry breaking

Ground-state symmetries are firstly investigated with the symmetry parameter ζ defined in Eq. (11). As shown in Fig. 1(a), ζ is displayed as a function of the coupling strength α for the logarithmic discretization factors $\Lambda = 1.01$ and 1.02 with the same low-energy cutoff $\omega_{\min} \approx 5 \times 10^{-5} \omega_c$. The spontaneous symmetry breaking is confirmed by the emergence of the abrupt jump from $\zeta = 1$ to 0 . The values of the critical point $\alpha_c = 1.01(1)$ and $1.03(2)$ are then estimated, in agreement with $\alpha_c = 1$. It indicates that the values of the logarithmic discretization factor Λ are already sufficiently close to 1 for the continuum limit $\Lambda \rightarrow 1$.

In Fig. 1(b), the transition boundary α_c is plotted against ω_{\min}/ω_c on a linear-log scale. The results of the linear discretization are also presented for the lowest frequency $\omega_{\min}/\omega_c > 0.0007$ from supplementary calculations with $\omega_k = (k/M)\omega_c$. All of the data collapse onto a single curve, further confirming that the cases with $\Lambda = 1.01$ and 1.02 belong to the quasi linear discretization, yielding a high dense Ohmic spectrum. Using the fitting with

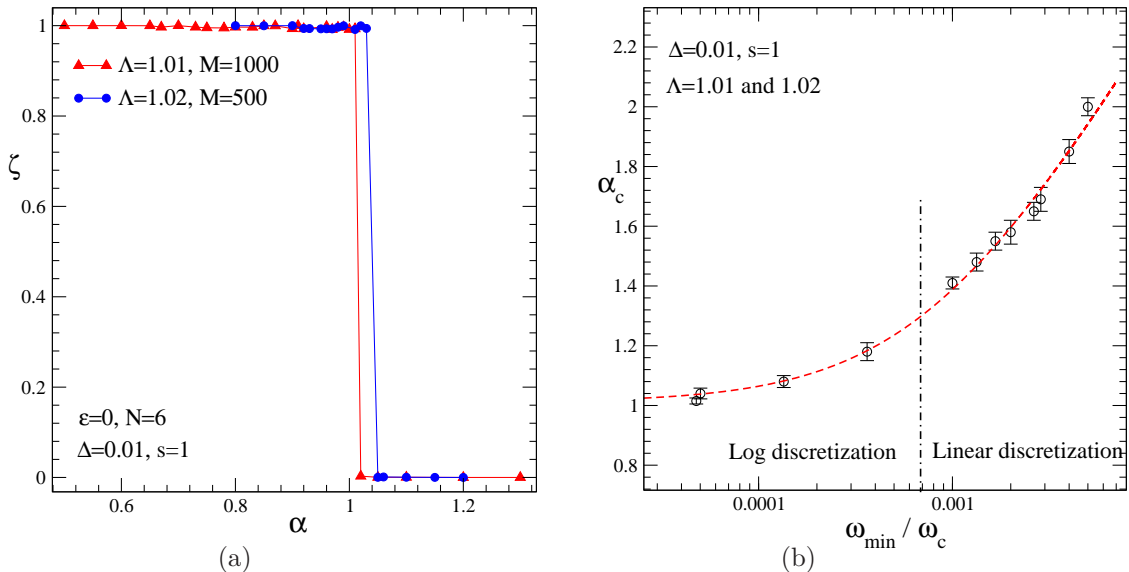


Figure 1: (a) The symmetry parameter ζ defined in Eq. (11) is plotted as a function of the coupling strength α on a linear scale. The tunneling amplitude $\Delta = 0.01$ and logarithmic discretization factor $\Lambda = 1.01$ and 1.02 are used for the Ohmic SBM at $s = 1$. (b) Displayed as a function of ω_{\min}/ω_c on a linear-log scale is the transition boundary α_c obtained from the symmetry parameter ζ . The results of the linear discretization are also given for $\omega_{\min}/\omega_c > 0.0007$. The dashed line represents the fit with a logarithmic form.

the logarithmic form $y = a \ln(x + b) + c$, the asymptotic value $\alpha_c = 1.0053$ is estimated by the extrapolation to $\omega_{\min} = 0$, consistent with the renormalization group prediction $\alpha_c = 1 + \mathcal{O}(\Delta/\omega_c)$ [5]. By a linear dependence on the tunneling amplitude Δ , one obtains the slope $(\alpha_c - 1)\omega_c/\Delta = 0.53$, in excellent agreement with the QMC one (0.5) estimated from $\alpha_c = 1.05$ at $\Delta = 0.1$ reported in Ref. [39]. Where the bath effects are taken into account by an effective Euclidean action whose kernel is expressed in terms of the continuous spectral density and bath propagator, instead of the discretization treatment of the Ohmic bath. Moreover, the prediction in this work for the frequency-range dependence of the critical coupling can be experimentally examined in the future.

For further understanding the symmetries, the average displacement coefficients \bar{f}_k and \bar{g}_k defined in Eq. (8) are measured at $\Lambda = 1.01$ and $M = 1000$ for different coupling strengths α and bath-mode frequencies ω_k , as shown in Fig. 2. Taking $\alpha = 0.5, 0.6, 0.7$ and 0.9 as examples, a perfect antisymmetry relation $\bar{f}_k = -\bar{g}_k$ is observed over the whole range of frequencies ω_k in the

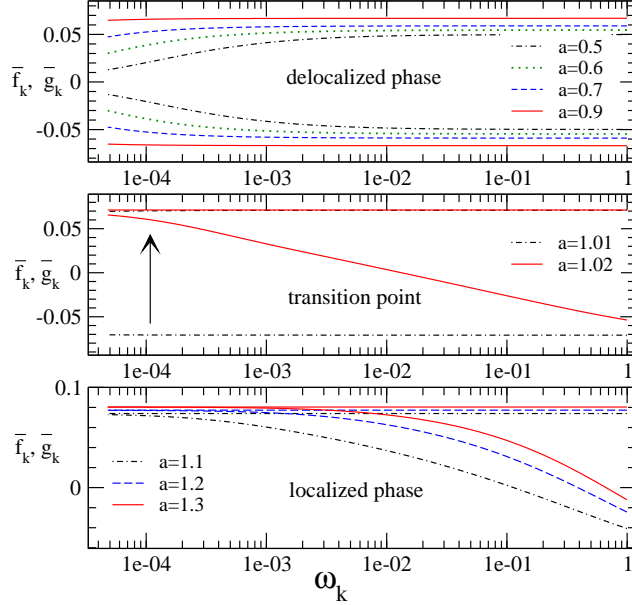


Figure 2: The average displacement coefficients \bar{f}_k and \bar{g}_k for different couplings α are plotted with solid, dashed, dotted, and dash-dotted lines on a linear-log scale. Different behaviors are found in three panels from top to bottom, corresponding to the delocalized phase, transition point, and localized phase, respectively. The arrow indicates a huge jump of the average displacement coefficients in the low-frequency regime.

upper panel, consistent with the usual assumption concerning the delocalized phase [17, 20]. For $\alpha = 1.1, 1.2$ and 1.3 , either \bar{f}_k or \bar{g}_k is equal to the classical displacement $\lambda_k/2\omega_k = \text{constant}$, hence pointing to the localized phase. In the middle panel, a huge jump appears in the low-frequency asymptotic value of the displacement coefficient (\bar{f}_k or \bar{g}_k) as the coupling strength α is changed by only a paltry amount of 0.01 . It again shows that the symmetry gets spontaneously broken at the critical coupling $\alpha_c = 1.01(1)$.

3.2. Quantum fluctuations and correlations

In this subsection, quantum fluctuations and correlations in the Ohmic bath are investigated for the Kosterlitz-Thouless transition. As single-coherent states obey minimum uncertainty relation $\Delta X_b = \Delta P_b = 1/2$, quantum fluctuation from the coherent superposition in Eq. (3) can be measured by the departure $\Delta X_b \Delta P_b - 1/4$. In Fig. 3(a), quantum fluctuation is plotted with respect to the frequency ω_k for various coupling strengths α on a log-log scale. It grows as a power law in the delocalized phase, e.g., $\Delta X_b \Delta P_b - 1/4 \sim \omega_k^2$ at

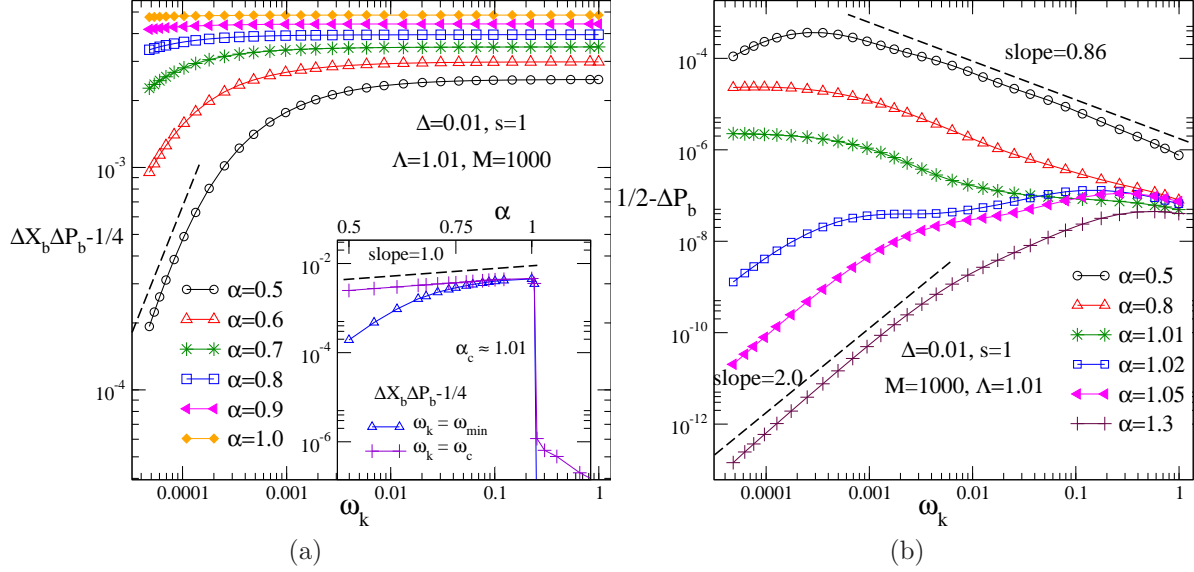


Figure 3: (a) The departure from the minimum uncertainty, $\Delta X_b \Delta P_b - 1/4$, is shown for different coupling strengths α as a function of the frequency ω_k on a log-log scale. In the inset, the asymptotic values of $\Delta X_b \Delta P_b - 1/4$ are plotted in the low- and high-frequency limits. (b) The quantum fluctuation $1/2 - \Delta P_b$ in the momentum space is displayed for different couplings α . In both (a) and (b), dashed lines represent power-law fits.

the Toulouse point $\alpha = 0.5$, and gradually approaches to a α -dependent constant value. Insets show the asymptotic values of the quantum fluctuations in the low- and high-frequency limits, taking the cases of $\omega_k = \omega_{\min}$ (solid line with open triangles) and $\omega_k = \omega_c$ (solid line with pluses) as examples. The transition point is located at $\alpha_c = 1.01(1)$ by the drop of $\Delta X_b \Delta P_b - 1/4$ from 10^{-2} to 10^{-6} . Moreover, the intersection of two curves suggests that the quantum fluctuation is independent of ω_k around the critical point α_c . In the delocalized phase with $\alpha < \alpha_c$, a clean power-law behavior is found in the high-frequency limit, and the slope 1.0 indicates that the saturation departure is proportional to the coupling. For the coupling $\alpha > \alpha_c$, the asymptotic values vanish in both two cases, confirming that the bath modes behave as a single-coherent state in the localized phase.

Quantum fluctuation of the momentum is also presented in Fig. 3(b) for different couplings α on a log-log scale. In contrast to $\Delta X_b \Delta P_b - 1/4$, the offset $1/2 - \Delta P_b$ in the delocalized phase shows a tendency to decay with the frequency ω_k . Especially at the Toulouse point $\alpha = 0.5$, a nice power-law decrease is found over more than three decades in frequencies,

and the slope $\eta = 0.86(1)$ is measured accurately. In the localized phase, the momentum fluctuation grows by more than four orders of magnitude, indicating that the value of $1/2 - \Delta P_b$ at the low frequency is negligibly small, as compared to those in the high-frequency region and in the delocalized phase. Besides, the slope 2.0 is the same as that of $\Delta X_b \Delta P_b - 1/4$, suggesting that the power-law growth of quantum fluctuation is trivial in both two phases. Interestingly, a flattened curve can be inferred between $\alpha = 1.01$ and 1.02, pointing again that the quantum fluctuation is frequency-independent at the transition point.

In the recent work [43], two strong fingerprints of quantum criticality have been reported in the sub-Ohmic SBM. One is an algebraic decay of the average displacement $\bar{f}_k \sim \omega_k^{(1-s)/2}$, and the other is a constant average squeezing amplitude which is related to the quantum fluctuation. In the Ohmic SBM with $s = 1$, both the fingerprints are verified through our numerical work where \bar{f}_k , $\Delta X_b \Delta P_b - 1/4$, and $1/2 - \Delta P_b$ are frequency-independent at the transition point, as shown in Figs. 2, and 3. In addition, a constant plateau of $\Delta X_b \Delta P_b - 1/4$ is found in the delocalized phase $\alpha < \alpha_c$ for the frequencies $\omega_k \geq \omega^*$, corresponding to the critical domain. It confirms that the Ohmic bath possesses the quantum criticality even in the delocalized phase. It is quite similar with those in the low-temperature phase of the classical two-dimensional XY model, embodying the universality of the Kosterlitz-Thouless transition [51]. Further analysis on the ground-state wave function gives that the above deviations from the minimum uncertainty relation $\Delta X_b = \Delta P_b = 1/2$ are mainly caused by the effects of the antipolaron states which take place naturally in the delocalized phase [20].

Besides quantum fluctuations, quantum correlations in the phase space, Cor_X and $-\text{Cor}_P$ defined in Eq. (5), are also investigated as a function of the coupling α and two frequencies ω_l and ω_k . Without loss of generality, the subscript $l = 0$ is fixed for convenience, corresponding to $\omega_l = \omega_{\min}$. Similar with $\Delta X_b \Delta P_b - 1/4$, quantum correlation Cor_X exhibits a smooth increase with the frequency ω_k . It is in contrast to the general consensus on traditional statistical models, that is, the correlation function decaying with the distance. The possible reason is that all of the bath modes in SBM are uncoupled but simultaneously interact with the common spin system. To exclude the contribution of quantum fluctuation, we introduce the correlation-fluctuation ratio function $R_{l=0} = \text{Cor}_X / (\Delta X_b - 1/2)$ instead.

As displayed in Fig. 4(a), the correlation-fluctuation ratio function $R_{l=0}$ decreases monotonically with increasing ω_k , and approaches a α -dependent

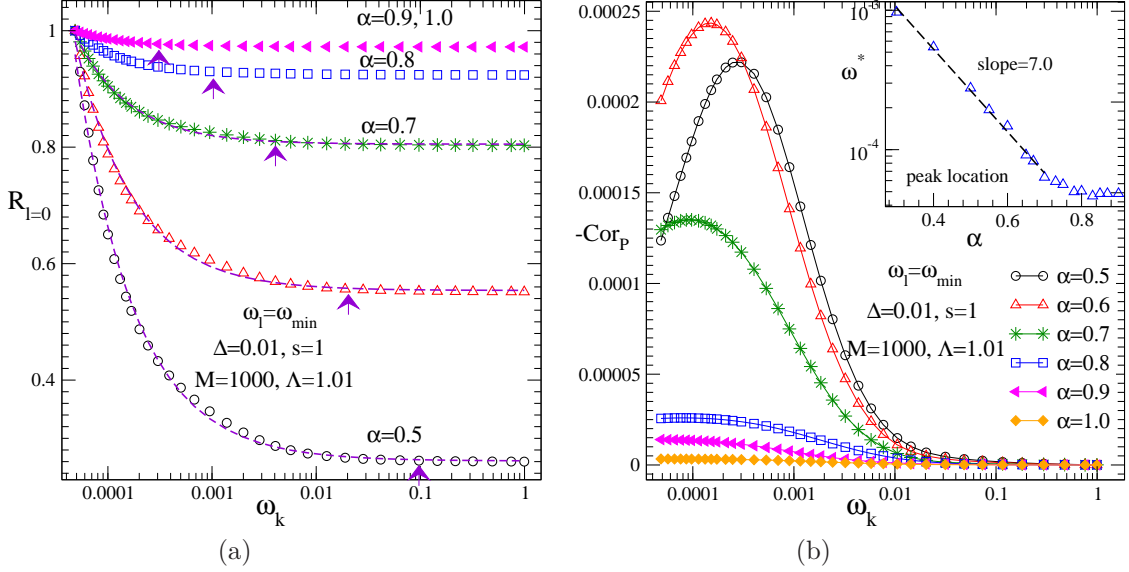


Figure 4: (a) The correlation-fluctuation ratio function $R_{l=0} = \text{Cor}_X / (\Delta X_b - 1/2)$ at the fixed frequency $\omega_l = \omega_{\min}$ is plotted as a function of the frequency ω_k and coupling strength α on a linear-log scale. Other parameters $\Delta = 0.01, s = 1, \Lambda = 1.01$, and $M = 1000$ are set. Dashed lines show the best fits for the power-law decays. The transition frequencies ω^* beyond which the constant plateaus appear are marked by the arrows. (b) The ω_k -dependent correlation function $-\text{Cor}_p$ is plotted on a linear-log scale. Inset shows the optimal frequency ω^* , and the dashed line represents an exponential fit.

constant. Dashed lines provide the power-law fitting to the numerical data, yielding the shift $\Delta R_{l=0} = R_{l=0}(\omega_k) - R_{l=0}(\omega_c) \sim \omega_k^{-\eta}$. The decaying exponent $\eta = 0.85(2)$ at $\alpha = 0.5$ agrees well with that in Fig. 3(b). Moreover, one observes the critical domain at high frequencies $\omega_k \geq \omega^*$, which gradually broadens into the whole frequency region as the coupling α increases, just the same as those of $\Delta X_b \Delta P_b - 1/4$. It indicates the correlation length $\xi = 1/\omega^*$ shows a tendency to diverge when α tends toward the critical coupling $\alpha_c = 1$. An exponential increase of ξ with the coupling α is then expected. In Fig. 4(b), the momentum correlation function $-\text{Cor}_p$ exhibits bell-shaped relation, and the position of the peak decays with the coupling as $\omega^* \sim \exp(-7.0\alpha)$ until it arrives at ω_{\min} when $\alpha > 0.8$, consistent with the previous prediction.

For comparison, quantum correlation Cor_X at another fixed frequency $\omega_l = \omega_c$ (i.e., $l = M$) is plotted in Fig. 5. For clarity, it is rescaled by a factor $1/\alpha$. One clearly observes that the curves of different α overlap at high

frequencies, confirming the linear coupling dependence of Cor_X , the same as that of $\Delta X_b \Delta P_b - 1/4$. Since the correlation-fluctuation ratio is $R_{l=M} \equiv 1$ at the cutoff frequency ω_c , inset shows the offset $R_{l=M} - 1$ as a function of ω_k for different coupling α on a log-log scale. It exhibits a power-law decay at the Toulouse point $\alpha = 0.5$, and the slope $\eta = 0.84(2)$ is again consistent with the one in Fig. 3(b). For the coupling strength close to the transition point, e.g., $\alpha = 1.0$ and the decay

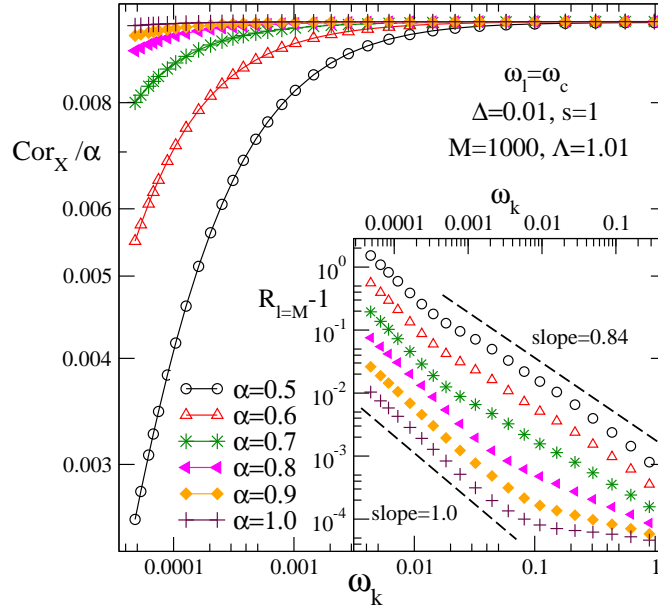


Figure 5: The scaled correlation function Cor_X/α is plotted at the fixed frequency $\omega_l = \omega_c$ as a function of the bosonic frequency ω_k for different values of α on a log-log scale. Other parameters $\Delta = 0.01, s = 1, \Lambda = 1.01$, and $M = 1000$ are set. Inset shows the correlation-fluctuation ratio function $R_{l=M} - 1$ with respect to ω_k and α . Dashed lines represent power-law fits.

3.3. Validity of variational calculations

The validity of the variational approach is carefully examined in this subsection. Firstly, the convergency test of the ground-state energy E_g is performed with respect to the numbers of the coherent superposition states N and effective bath modes M defined in Eq. (3), taking the case of $\alpha = 1, \Delta = 0.01$, and $\Lambda = 1.01$ as an example. In Fig.6(a), the energy shift

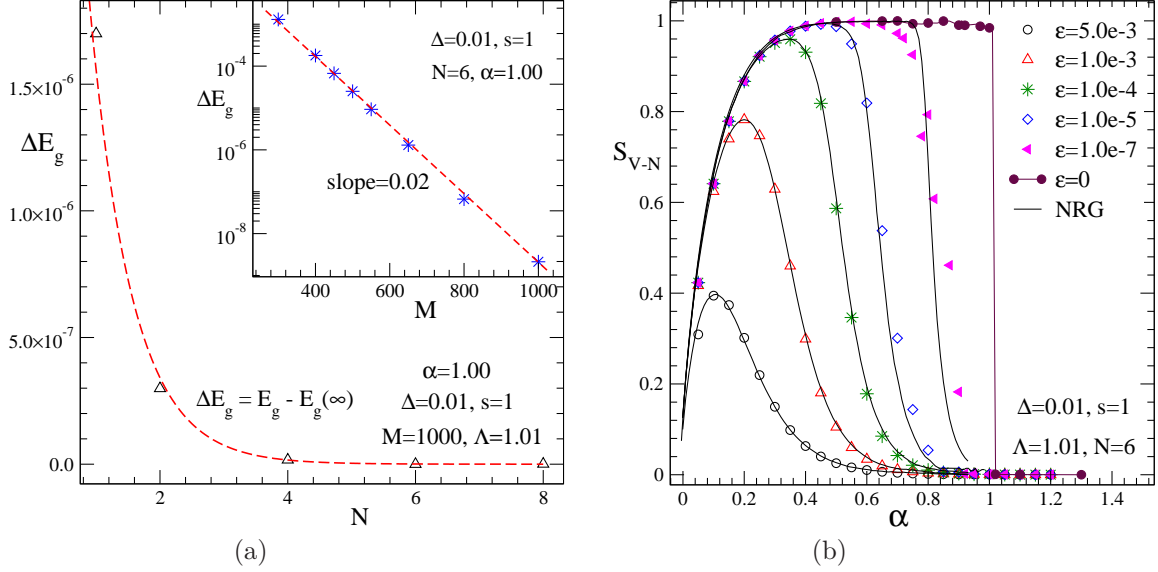


Figure 6: (a) The convergence of ground-state energy E_g is displayed with respect to the numbers of the coherent superposition states N and effective bath modes M (in the inset) in the case of $s = 1, \alpha = 1, \Delta = 0.01$, and $\Lambda = 1.01$. Dashed lines show exponential fits to the ground-state energy shift $\Delta E_g = E_g - E_g(\infty)$. (b) The von Neumann entropy S_{V-N} is plotted as a function of α for different values of the bias $\epsilon = 0.005, 10^{-3}, 10^{-4}, 10^{-5}, 10^{-7}$ and 0 (from left to right). For comparison, the results of NRG calculations are also shown with solid lines.

$\Delta E_g = E_g(N) - E_g(\infty)$ is shown for a fixed parameter $M = 1000$ on a linear scale, where $E_g(\infty)$ is the asymptotic value of the ground-state energy. As α increases, the shift decays exponentially as $\Delta E_g \sim \exp(-1.5N)$. The significantly large slope suggests that a small value of N , i.e., $N = 6$, is sufficient to study the ground-state phase transitions of Ohmic SBM via the variational approach. Moreover, the dependence of ΔE_g on the bath-mode number M is demonstrated in the inset of Fig.6(a) on a linear-log scale at $N = 6$. Similarly, an exponential decay of ΔE_g is observed with the slope 0.02, showing that $M = 1000$ is sufficient for the convergence.

Subsequently, extension to the biased Ohmic SBM is performed for the spin-related observations, such as the spin magnetization $\langle \sigma_z \rangle$, spin coherence $\langle \sigma_x \rangle$, and von-Neumann entropy S_{V-N} which denotes the entanglement between the spin and surrounding bath, $S_{V-N} = -\omega_+ \log \omega_+ - \omega_- \log \omega_-$ where $\omega_{\pm} = (1 \pm \sqrt{\langle \sigma_x \rangle^2 + \langle \sigma_y \rangle^2 + \langle \sigma_z \rangle^2})/2$. For comparison, the results of NRG calculations are also given with the parameters, e.g., logarithmic discretiza-

tion factor $\Lambda = 2$, lowest energy levels $N_s = 150$, and bosonic truncated number $N_b = 8$, the same as those in the earlier work [52].

Taking the von-Neumann entropy S_{v-N} presented in Fig. 6(b) as a representative example, the results of NVM and NRG approaches agree well for the biases $\varepsilon = 0.005, 10^{-3}, 10^{-4}$, and 10^{-5} , although there is a slight deviation under a weaker bias $\varepsilon = 1.0 \times 10^{-7}$. It indicates that both of these two approaches are available to obtain an accurate description of the ground state. In addition, an infinitesimal but nonvanishing bias is usually used in NRG calculations to lift the degeneracy [29]. Even under a tiny bias $\varepsilon = 1.0 \times 10^{-7}$, however, a sharp crossover occurs instead of the discontinuity, and the transition point estimated from the abrupt jump of NRG curve is obviously smaller than $\alpha_c = 1$, as shown in the subfigure. In contrast, the value of $\alpha_c = 1.01(1)$ from NVM calculations with the vanishing bias $\varepsilon = 0$ is consistent with the theoretical prediction $\alpha_c \rightarrow 1^+$, thereby lending support to the superiority of the variational calculations.

4. Conclusion

By performing large-scale numerical variational calculations with a quasi-linear discretization, we have presented a comprehensive study of the ground-state quantum phase transitions of Ohmic SBM in a high dense spectrum in the weak tunneling limit, using the bare tunneling amplitude $\Delta = 0.01$ and discretization factor $\Lambda = 1.01$. The asymptotic value of the critical coupling $\alpha_c = 1.0053$ has been accurately determined by extrapolation to $\omega_{\min} = 0$, in good agreement with the theoretical prediction $\alpha_c = 1 + \mathcal{O}(\Delta/\omega_c)$ [5] and very recent numerical results obtained by the imaginary-time propagation [38, 39]. The values of the exponent $\eta = 0.85(2)$ and 0 have been measured from the quantum fluctuations and correlations in the Ohmic bath at the Toulouse point $\alpha = 0.5$ and transition point α_c , respectively. In addition, quantum criticality of Ohmic bath has been demonstrated explicitly both in the delocalized phase and at the transition point, lending support to the quantum phase transition of the Kosterlitz-Thouless type.

Very recently, quantum simulations of the spin-boson model have been realized by using a superconducting qubit connected to a microwave circuit wherein the tunability of the interaction allows one to observe quantum phase transitions [16, 53]. Our work provides the prediction on the ω_{\min} dependence of the transition point which can be experimental examined in the future,

and the guidance for the choices of the Ohmic-bath frequency range ω_c/ω_{\min} in experiments to achieve the exact transition point $\alpha_c = 1$.

Acknowledgements: This work was supported in part by National Natural Science Foundation of China under Grant Nos. 11875120.

References

References

- [1] U. Weiss, Quantum Dissipative Systems, 3rd Edition, World Scientific, Singapore, 2007.
- [2] K. L. Hur, CRC Press, Boca Raton, 2010, Ch. 9, pp. 217–240.
- [3] S. Sachdev, Quantum Phase Transitions, 2nd Edition, Cambridge University Press, Cambridge, England, 2011.
- [4] A. J. Leggett, S. Chakravarty, A. T. Dorsey, M. P. A. Fisher, A. Garg, W. Zwerger, Dynamics of the dissipative two-state system, *Rev. Mod. Phys.* 59 (1987) 1–85. doi:10.1103/RevModPhys.59.1.
- [5] K. L. Hur, Entanglement entropy, decoherence, and quantum phase transitions of a dissipative two-level system, *Annals of Physics* 323 (2008) 2208 – 2240. doi:10.1016/j.aop.2007.12.003.
- [6] H. P. Breuer, E. M. Laine, J. Piilo, B. Vacchini, Colloquium: Non-markovian dynamics in open quantum systems, *Rev. Mod. Phys.* 88 (2016) 021002. doi:10.1103/RevModPhys.88.021002.
- [7] J. T. Lewis, G. A. Raggio, The equilibrium thermodynamics of a spin-boson model, *J. Stat. Phys* 50 (1988) 1201. doi:10.1007/BF01019161.
- [8] B. Golding, N. M. Zimmerman, S. N. Coppersmith, Dissipative quantum tunneling of a single microscopic defect in a mesoscopic metal, *Phys. Rev. Lett.* 68 (1992) 998–1001. doi:10.1103/PhysRevLett.68.998.
- [9] S. Chakravarty, J. Rudnick, Dissipative dynamics of a two-state system, the kondo problem, and the inverse-square ising model, *Phys. Rev. Lett.* 75 (1995) 501–504. doi:10.1103/PhysRevLett.75.501.

- [10] G. S. Engel, T. R. Calhoun, E. L. Read, T. K. Ahn, T. Mancal, Y. C. Cheng, R. E. Blankenship, G. R. Fleming, Evidence for wavelike energy transfer through quantum coherence in photosynthetic systems, *Nature* 446 (2007) 782–786. doi:10.1038/nature05678.
- [11] E. Collini, G. D. Scholes, Coherent intrachain energy migration in a conjugated polymer at room temperature, *Science* 323 (2009) 369–373. doi:10.1126/science.1164016.
- [12] L. Garbe, I. L. Egusquiza, E. Solano, C. Ciuti, T. Coudreau, P. Milman, S. Felicetti, Superradiant phase transition in the ultrastrong-coupling regime of the two-photon dicke model, *Phys. Rev. A* 95 (2017) 053854. doi:10.1103/PhysRevA.95.053854.
- [13] Y. Ota, S. Iwamoto, N. Kumagai, Y. Arakawa, Spontaneous two-photon emission from a single quantum dot, *Phys. Rev. Lett.* 107 (2011) 233602. doi:10.1103/PhysRevLett.107.233602.
- [14] D. Porras, F. Marquardt, J. von Delft, J. I. Cirac, Mesoscopic spin-boson models of trapped ions, *Phys. Rev. A* 78 (2008) 010101(R). doi:10.1103/PhysRevA.78.010101.
- [15] R. Uzdin, A. Levy, R. Kosloff, Equivalence of quantum heat machines, and quantum-thermodynamic signatures, *Phys. Rev. X* 5 (2015) 031044. doi:10.1103/PhysRevX.5.031044.
- [16] J. Leppäkangas, J. Braumüller, M. Hauck, J.-M. Reiner, I. Schwenk, S. Zanker, L. Fritz, A. V. Ustinov, M. Weides, M. Marthaler, Quantum simulation of the spin-boson model with a microwave circuit, *Phys. Rev. A* 97 (2018) 052321. doi:10.1103/PhysRevA.97.052321.
- [17] R. Silbey, R. A. Harris, Variational calculation of the dynamics of a two level system interacting with a bath, *J. Chem. Phys.* 80 (1984) 2615–2617. doi:10.1063/1.447055.
- [18] A. W. Chin, J. Prior, S. F. Huelga, M. B. Plenio, Generalized polaron ansatz for the ground state of the sub-ohmic spin-boson model: An analytic theory of the localization transition, *Phys. Rev. Lett.* 107 (2011) 160601. doi:10.1103/PhysRevLett.107.160601.

- [19] A. Nazir, D. P. S. McCutcheon, A. W. Chin, Ground state and dynamics of the biased dissipative two-state system: Beyond variational polaron theory, *Phys. Rev. B* 85 (2012) 224301. doi:10.1103/PhysRevB.85.224301.
- [20] S. Bera, A. Nazir, A. W. Chin, H. U. Baranger, S. Florens, Generalized multipolaron expansion for the spin-boson model: Environmental entanglement and the biased two-state system, *Phys. Rev. B* 90 (2014) 075110. doi:10.1103/PhysRevB.90.075110.
- [21] W. Wu, J. B. Xu, Quantum coherence of spin-boson model at finite temperature, *Annals of Physics* 377 (2017) 48 – 61. doi:https://doi.org/10.1016/j.aop.2017.01.014.
- [22] M. Pino, J. J. García-Ripoll, Quantum annealing in spin-boson model: from a perturbative to an ultrastrong mediated coupling, *New Journal of Physics* 20 (2018) 113027. doi:10.1088/1367-2630/aaeeea.
- [23] P. Nalbach, M. Thorwart, Crossover from coherent to incoherent quantum dynamics due to sub-ohmic dephasing, *Phys. Rev. B* 87 (2013) 014116. doi:10.1103/PhysRevB.87.014116.
- [24] C. Guo, A. Weichselbaum, J. von Delft, M. Vojta, Critical and strong-coupling phases in one- and two-bath spin-boson models, *Phys. Rev. Lett.* 108 (2012) 160401. doi:10.1103/PhysRevLett.108.160401.
- [25] N. J. Zhou, L. P. Chen, Y. Zhao, D. Mozyrsky, V. Chernyak, Y. Zhao, Ground-state properties of sub-ohmic spin-boson model with simultaneous diagonal and off-diagonal coupling, *Phys. Rev. B* 90 (2014) 155135. doi:10.1103/PhysRevB.90.155135.
- [26] N. J. Zhou, Y. Y. Zhang, Z. G. Lü, Y. Zhao, Variational study of the two-impurity spin-boson model with a common ohmic bath: Ground-state phase transitions, *Annalen der Physik* 530 (2018) 1800120. doi:10.1002/andp.201800120.
- [27] Y. Z. Wang, S. He, L. W. Duan, Q. H. Chen, Rich phase diagram of quantum phases in the anisotropic subohmic spin-boson model, *Phys. Rev. B* 101 (2020) 155147. doi:10.1103/PhysRevB.101.155147.

- [28] F. Guinea, V. Hakim, A. Muramatsu, Bosonization of a two-level system with dissipation, *Phys. Rev. B* 32 (1985) 4410–4418. doi:10.1103/PhysRevB.32.4410.
- [29] P. P. Orth, D. Roosen, W. Hofstetter, K. Le Hur, Dynamics, synchronization, and quantum phase transitions of two dissipative spins, *Phys. Rev. B* 82 (2010) 144423. doi:10.1103/PhysRevB.82.144423.
- [30] D. P. S. McCutcheon, A. Nazir, S. Bose, A. J. Fisher, Separation-dependent localization in a two-impurity spin-boson model, *Phys. Rev. B* 81 (2010) 235321. doi:10.1103/PhysRevB.81.235321.
- [31] A. Winter, H. Rieger, Quantum phase transition and correlations in the multi-spin-boson model, *Phys. Rev. B* 90 (2014) 224401. doi:10.1103/PhysRevB.90.224401.
- [32] L. Magazzù, P. Forn-Díaz, R. Belyansky, J.-L. Orgiazzi, M. A. Yurtalan, M. R. Otto, A. Lupascu, C. M. Wilson, M. Grifoni, Probing the strongly driven spin-boson model in a superconducting quantum circuit, *Nature Communications* 9 (2018) 1403. doi:10.1038/s41467-018-03626-w.
- [33] M. Vojta, N. H. Tong, R. Bulla, Quantum phase transitions in the sub-ohmic spin-boson model: Failure of the quantum-classical mapping, *Phys. Rev. Lett.* 94 (2005) 070604. doi:10.1103/PhysRevLett.94.070604.
- [34] A. Alvermann, H. Fehske, Sparse polynomial space approach to dissipative quantum systems: Application to the sub-ohmic spin-boson model, *Phys. Rev. Lett.* 102 (2009) 150601. doi:10.1103/PhysRevLett.102.150601.
- [35] A. Winter, H. Rieger, M. Vojta, R. Bulla, Quantum phase transition in the sub-ohmic spin-boson model: Quantum monte carlo study with a continuous imaginary time cluster algorithm, *Phys. Rev. Lett.* 102 (2009) 030601. doi:10.1103/PhysRevLett.102.030601.
- [36] Y. Y. Zhang, Q. H. Chen, K. L. Wang, Quantum phase transition in the sub-ohmic spin-boson model: An extended coherent-state approach, *Phys. Rev. B* 81 (2010) 121105(R). doi:10.1103/PhysRevB.81.121105.

- [37] R. Bulla, H. J. Lee, N. H. Tong, M. Vojta, Numerical renormalization group for quantum impurities in a bosonic bath, *Phys. Rev. B* 71 (2005) 045122. doi:10.1103/PhysRevB.71.045122.
- [38] H. Wang, J. Shao, Quantum phase transition in the spin-boson model: A multilayer multiconfiguration time-dependent hartree study, *J. Phys. Chem. A* 123 (2019) 1882–1893. doi:10.1021/acs.jpca.8b11136.
- [39] G. De Filippis, A. de Candia, L. M. Cangemi, M. Sasseti, R. Fazio, V. Cataudella, Quantum phase transitions in the spin-boson model: Monte carlo method versus variational approach à la feynman, *Phys. Rev. B* 101 (2020) 180408(R). doi:10.1103/PhysRevB.101.180408.
- [40] H. Zheng, Z. G. Lü, Y. Zhao, Ansatz for the quantum phase transition in a dissipative two-qubit system, *Phys. Rev. E* 91 (2015) 062115. doi:10.1103/PhysRevE.91.062115.
- [41] S. Florens, I. Snyman, Universal spatial correlations in the anisotropic kondo screening cloud: Analytical insights and numerically exact results from a coherent state expansion, *Phys. Rev. B* 92 195106. doi:10.1103/PhysRevB.92.195106.
- [42] S. He, L. W. Duan, Q. H. Chen, Improved silbey-harris polaron ansatz for the spin-boson model, *Phys. Rev. B* 97 (2018) 115157. doi:10.1103/PhysRevB.97.115157.
- [43] Z. Blunden-Codd, S. Bera, B. Bruognolo, N. O. Linden, A. W. Chin, J. von Delft, A. Nazir, S. Florens, Anatomy of quantum critical wave functions in dissipative impurity problems, *Phys. Rev. B* 95 (2017) 085104. doi:10.1103/PhysRevB.95.085104.
- [44] N. J. Zhou, L. P. Chen, D. Z. Xu, V. Chernyak, Y. Zhao, Symmetry and the critical phase of the two-bath spin-boson model: Ground-state properties, *Phys. Rev. B* 91 (2015) 195129. doi:10.1103/PhysRevB.91.195129.
- [45] N. J. Zhou, Z. K. Huang, J. F. Zhu, V. Chernyak, Y. Zhao, Polaron dynamics with a multitude of davydov d2 trial states, *J. Chem. Phys.* 143 (2015) 014113. doi:10.1063/1.4923009.

- [46] N. J. Zhou, L. P. Chen, Z. K. Huang, K. W. Sun, Y. Tanimura, Y. Zhao, Fast, accurate simulation of polaron dynamics and multidimensional spectroscopy by multiple davydov trial states, *J. Phys. Chem. A* 120 (2016) 1562–1576. doi:10.1021/acs.jpca.5b12483.
- [47] L. Wang, L. P. Chen, N. J. Zhou, Y. Zhao, Variational dynamics of the sub-ohmic spin-boson model on the basis of multiple davydov d1 states, *J. Chem. Phys.* 144 (2016) 024101. doi:10.1063/1.4939144.
- [48] L. Wang, Y. Fujihashi, L. P. Chen, Y. Zhao, Finite-temperature time-dependent variation with multiple davydov states, *J. Chem. Phys.* 146 (2017) 124127. doi:10.1063/1.4979017.
- [49] R. Bulla, N. H. Tong, M. Vojta, Numerical renormalization group for bosonic systems and application to the sub-ohmic spin-boson model, *Phys. Rev. Lett.* 91 (2003) 170601. doi:10.1103/PhysRevLett.91.170601.
- [50] M. F. Frenzel, M. B. Plenio, Matrix product state representation without explicit local hilbert space truncation with applications to the sub-ohmic spin-boson model, *New J. Phys.* 15 (7) (2013) 073046.
- [51] J. M. Kosterlitz, The critical properties of the two-dimensional xy model, *J. Phys. C: Solid State Phys.* 7 (6) (1974) 1046.
- [52] K. Le Hur, P. Doucet-Beaupré, W. Hofstetter, Entanglement and criticality in quantum impurity systems, *Phys. Rev. Lett.* 99 (2007) 126801. doi:10.1103/PhysRevLett.99.126801.
- [53] T. Yamamoto, T. Kato, Microwave scattering in the subohmic spin-boson systems of superconducting circuits, *J. Phys. Soc. Jpn.* 88 (2019) 094601. doi:10.7566/JPSJ.88.094601.